

Times of Emission of K X Rays from Cf^{252} Fission Fragments of Known Mass* †

A. B. LONG, ‡ B. W. WEHRING, AND M. E. WYMAN

Nuclear Engineering Program, University of Illinois, Urbana, Illinois 61801

(Received 13 June 1969)

The measured yield of K x rays emitted from fission fragments of Cf^{252} is reported as a function of the time after fission for times between 1 and 56 nsec, and as a function of the mass of the fragment emitting the x ray. In the experiment, three-parameter data were recorded event by event. The first and second parameters contained information about the energies of both fission fragments from which it was possible to calculate the mass of each fragment. The third parameter contained a signal that was proportional to the time that elapsed between the detection of one of the fission fragments and the detection of an x ray. The timing data were sorted to yield x-ray timing spectra for fission-fragment mass intervals 4 amu wide. Each timing spectrum was fitted with a function that was derived from folding the prompt-response function of the system into a sum of three exponential decays. This analytical technique permitted the determination of the percent of the total x-ray emissions coming from each of the three half-life groups. These results, in conjunction with the yield data, were then interpreted in terms of fragment excitation states and comparisons were made with previously reported data.

I. INTRODUCTION

SUBSEQUENT to the act of fissioning, the highly excited fission fragments deexcite first by the emission of neutrons and then through the process of γ decay. Frequently, one of the lower-energy γ transitions will internally convert in the K shell. The electron vacancy produced in this manner is filled promptly ($< 10^{-16}$ sec) by an outer-shell electron, often with the resulting emission of a K x ray. In the present work, the times of emission of these x rays were studied with respect to the mass of the fragment emitting the x ray and with respect to the total kinetic energy imparted to the two fragments. Because the timing region investigated lay between 1 and 56 nsec after fission, and because the x-ray emission occurs so promptly after internal conversion, it was possible to interpret the x-ray timing data in terms of the nuclear transition times. When combined with data on x-ray yields, these results provide information about the excited energy states in fission-fragment nuclei.

Most of the recent experiments dealing with K x rays emitted by fission fragments have been concerned with determining the atomic-number distribution of the fission fragments.¹⁻⁵ Only Kapoor, Bowman, and Thompson,¹ and Dolce, Gibson, and Thomas⁶ have reported results in which the times of emission of

x rays were measured as a function of the fragment mass. In both of these experiments an average time of emission was calculated as a function of fragment mass. In the present experiment, detailed x-ray timing spectra were recorded for the different fission-fragment-mass and kinetic-energy intervals and were then fitted with a function that was derived from folding the prompt-response function of the system into a sum of exponential decays. This analytical technique permitted the determination of the relative amounts of the different half-life groups present in each of the spectra.

II. EXPERIMENTAL SYSTEM

A. Apparatus

The present experiment was designed to measure the time after fission at which a K x ray was emitted by a fission fragment, and to measure the kinetic energy and mass of that fission fragment. The time of x-ray emission after fission was determined by a time-to-pulse-height converter from the overlap of two standard pulses, one generated upon detection of a fission fragment and the other upon detection of an x ray.

A cross-sectional diagram of the detector configuration is shown in Fig. 1. The Cf^{252} fission source consisted of a $90\text{-}\mu\text{g}/\text{cm}^2$ -thick nickel foil on which a source of 1332 fissions/sec had been self-transferred. Two Ortec 400-mm^2 -silicon surface-barrier detectors, which were collimated in order to minimize edge effects, served as the fission-fragment detectors. Both fission-fragment detectors and the fission foil were mounted on the end of the cylinder housing the x-ray detector. This entire unit was slipped into a vacuum chamber until a flange on the housing abutted with the end of the chamber to form a vacuum seal. The x-ray detector consisted of a 1-mm-thick $\text{NaI}(\text{Tl})$ crystal that had a 2.2-cm diam mounted on a thin quartz light pipe, which was in turn mounted on the end of a fast 56 AVP phototube. The crystal was covered by a 0.13-mm-thick Be window.

A copper and lead shield was placed between the

* Work supported by the National Science Foundation.

† Based upon a dissertation by one of the authors (ABL) submitted in partial fulfillment of the requirements for the doctoral degree at the University of Illinois.

‡ Former National Science Foundation Trainee. Present address: Reactor Physics Division, Argonne National Laboratory, Argonne, Ill.

¹ S. S. Kapoor, H. R. Bowman, and S. G. Thompson, *Phys. Rev.* **140**, B1310 (1965).

² L. E. Glendenin and J. P. Unik, *Phys. Rev.* **140**, B1301 (1965).

³ E. M. Bohn, B. W. Wehring, and M. E. Wyman, *Appl. Phys. Letters* **12**, 199 (1968).

⁴ B. W. Wehring and M. E. Wyman, *Phys. Rev.* **157**, 1083 (1967).

⁵ R. L. Watson, H. R. Bowman, and S. G. Thompson, *Phys. Rev.* **162**, 1169 (1967).

⁶ S. R. Dolce, W. M. Gibson, and T. D. Thomas (private communication).

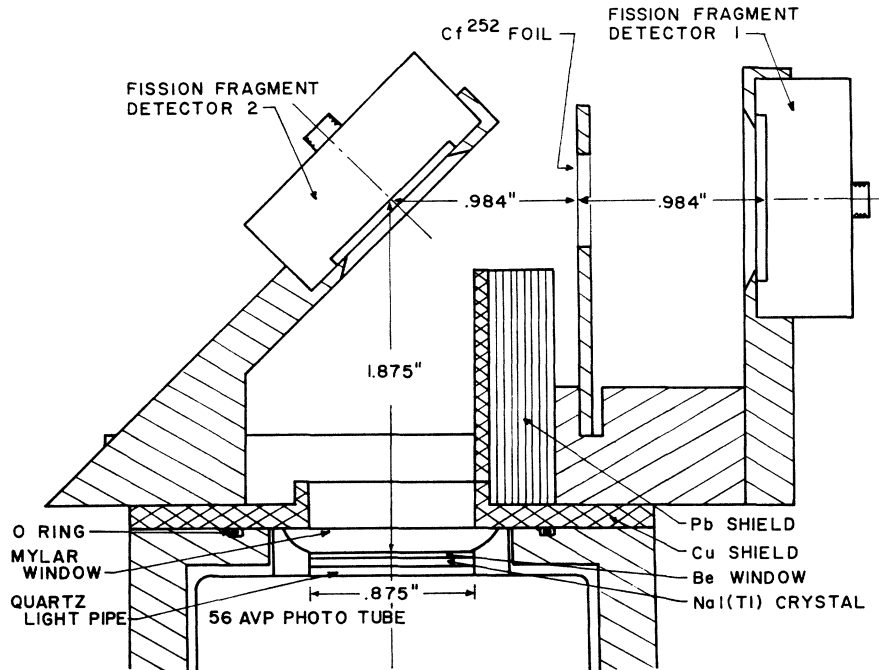


FIG. 1. Cross-sectional diagram of the detector configuration.

Cf^{252} foil and the x-ray detector in order to shield the detector from prompt and accidental radiation emanating from the Cf^{252} foil, and from any x rays emitted by the fission fragment moving towards detector 1. In addition, the first centimeter of the second fragment's flight path was also blocked from the view of the x-ray detector. For this reason it was not until approximately 1 nsec after fission that x rays emitted by the second fragment could be detected. An analysis of all possible fragment paths from the fission source to fission-fragment detector 2 showed that, as the fragment moved into view of the x-ray detector, the solid angle for x-ray detection increased from 10% to 90% of its final value in 0.3 nsec. The fractional solid angle for x-ray detection was 0.0118 ± 0.0018 when all the fragments stopped in the detector (~ 3 nsec after fission).

B. Electronics

A schematic diagram of the electronic equipment that is associated with the experiment is shown in

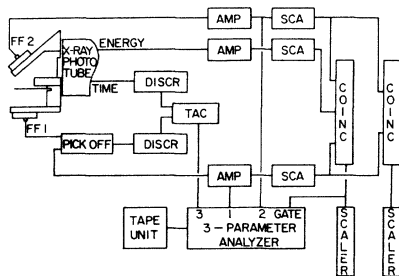


FIG. 2. Schematic diagram of the electronics associated with the experiment.

Fig. 2. A time-to-pulse-height converter measured the time between the detection of a fission fragment in detector 1 and the detection of an x ray using the overlap of two standard discriminator pulses, each of 90-nsec duration. The first discriminator was triggered by a time pickoff, which in turn had been triggered by the leading edge of the current pulse that was produced from the detection of a fission fragment in surface-barrier detector 1. The second discriminator was triggered by the fast timing signal that was generated at the anode of the photomultiplier tube from the detection of an x ray.

The slow electronics was composed of the two fission-fragment energy channels, and the x-ray energy channel, each of which consisted of conventional preamplifiers, double-delay-line amplifiers and single-channel analyzers. The energies of both fission fragments, plus the timing signal from the time-to-pulse-height converter, were presented to the three-parameter data acquisition system. This information was recorded by the system if a gate signal was generated by the triple-coincidence system from the detection of two fission fragments and a 5-48-keV x ray within the resolving time of $2\tau = 1.2 \mu\text{sec}$. When the memory of the data acquisition system was filled, the information was transferred to magnetic tape and later analyzed on an IBM 7094 computer.

The triple-coincidence counting rate for this detector arrangement was 0.101 triple-coincident events per second. The background-coincidence counting rate was one-sixth of the total coincidence rate, as was determined by placing a 0.8-mm-thick copper disk over the front of the x-ray detector. This thickness of copper absorbed essentially all of the x rays with energies

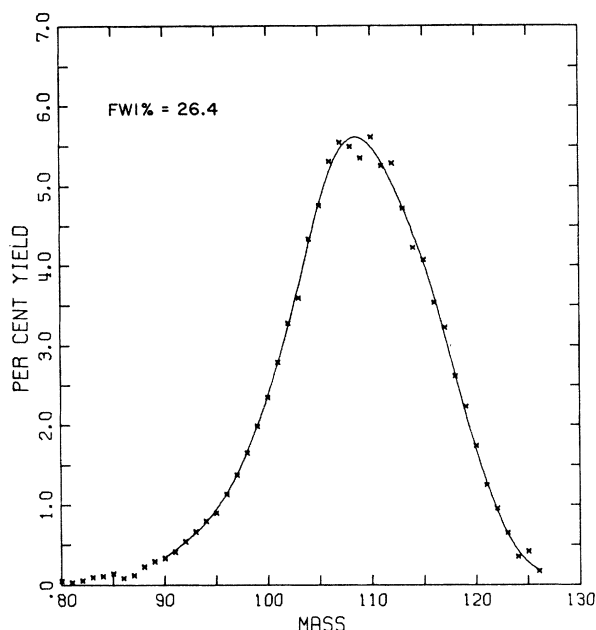


FIG. 3. Pre-neutron-emission mass distribution from the spontaneous fission of Cf^{252} . The plotted points are the values measured in run 38 of the experiment and the solid line was generated by two fourth-order power series fitted to both sides of the distribution and a fifth-order power series fitted to the peak.

below 48 keV, while allowing the higher-energy γ rays and neutrons to pass through.

III. DATA ANALYSIS AND RESULTS

A. Mass Determination

The pre-neutron-emission mass m_2^* of the fragment emitting the x ray was calculated from the pulse heights recorded for both fission fragments using an iterative technique. Estimating a value for m_2^* , and thus for m_1^* , the measured pulse heights were first corrected for pulse defect using the procedure developed by Schmitt.⁷ The resulting post-neutron-emission energies of both fragments, E_1 and E_2 , and the initial guess for pre-

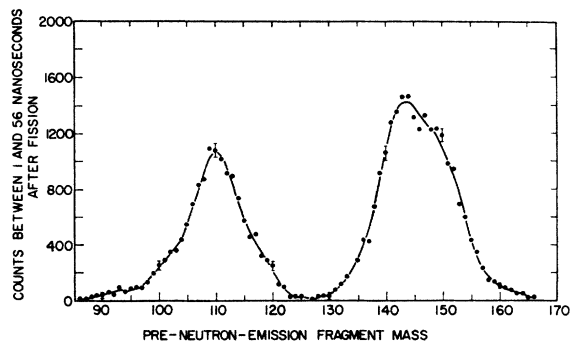


FIG. 4. Total x-ray counts recorded for times between 1 and 56 nsec after fission of Cf^{252} . The solid line was generated by least-squares fitting a 14th-order power series to each of the peaks.

⁷H. W. Schmitt, W. E. Kiker, and C. W. Williams, Phys. Rev. **137**, B837 (1965).

neutron-emission fragment masses were then used in Eq. (1) to determine a new value for m_2^* .

$$m_2^* = A E_1 / \left[E_1 + E_2 \left(\frac{1 - \bar{\nu}_1 / m_1^*}{1 - \bar{\nu}_2 / m_2^*} \right) \right], \quad (1)$$

where $\bar{\nu}_1$ and $\bar{\nu}_2$ are the average number of neutrons emitted by fragments of mass m_1^* and m_2^* , respectively, averaged over their kinetic energies as reported by Bowman *et al.*⁸ The effect of this approximation on mass dispersion was included in the mass-resolution analysis that is mentioned below. If the new value of m_2^* was not within 0.1 amu of the preceding value, the values were averaged and another iteration performed. Similar methods for calculating the masses of the fragments have been reported by Bohn⁹ and Schmitt.¹⁰

In order to ensure that the fission-fragment detectors and the associated electronics were functioning properly, double-fragment kinetic-energy calibration runs were made periodically throughout the experiment.¹¹ A

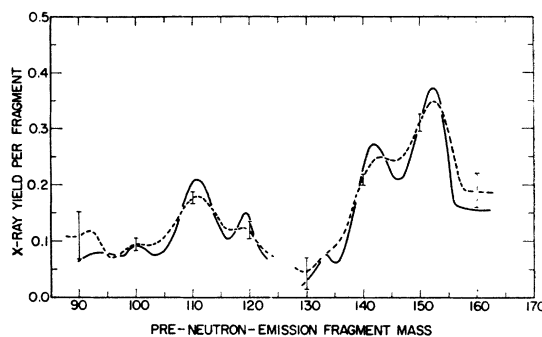


FIG. 5. X-ray yields per fragment for times between 1 and 56 nsec after fission of Cf^{252} . The solid line represents results corrected for mass dispersion. The dashed line represents uncorrected results.

typical Cf^{252} mass distribution containing 50 000 double-coincident events is shown plotted in Fig. 3. The solid curve was generated by the least-squares fitting of a fifth-order power series to the peak of the distribution and fourth-order power series to each side. The mass resolution of the system was then found by comparing the full width at 1% of the fitted data with values reported by Bohn *et al.*,⁹ for which the mass resolution had been calculated. In the case of this run, which was typical of those made during the experiment, the variance in mass was 5.1 amu².

B. X-Ray Yields

1. Procedure

To determine the x-ray yields per fragment between 1 and 56 nsec after fission, it was necessary to sum the

⁸H. R. Bowman, J. C. D. Milton, S. G. Thompson, and W. J. Swiatecki, Phys. Rev. **129**, 2123 (1963).

⁹E. M. Bohn, A. B. Long, R. D. Rollins, B. W. Wehring, and M. E. Wyman (unpublished).

¹⁰H. M. Schmitt, J. H. Neiler, and F. J. Walter, Phys. Rev. **141**, 1146 (1966).

¹¹A. B. Long, B. W. Wehring, and M. E. Wyman, Rev. Sci. Instr. **39**, 1566 (1968).

number of x rays emitted per nsec for each mass interval (1 amu) over the total time range observed in this experiment. Background x-ray yields for the same time interval were measured for each mass interval. In Fig. 4 the measured counts corrected for background are plotted versus the pre-neutron-emission mass of the fragment. The solid line was generated for each of the peaks by fitting a 14th-order power series to the data in that peak.

The fitted x-ray data were then corrected for the x-ray-detection solid angle, for the efficiency of the NaI detector, and for the absorption of x rays emitted by fragments that had penetrated into the detector. The latter two correction factors were calculated as a function of the most probable K x-ray energy corresponding to a given mass fragment. This energy was determined from Glendenin's data² on the most probable Z for a given fragment mass, and from Wapstra's data¹² on the average K x-ray energy associated with a given Z nucleus. The product of the two correction factors was then dispersed to account for the mass resolution of the system.

Finally, using a method suggested by Terrell,¹³ which also has been used by a number of other authors in the correction of their x-ray yields,^{1,6} the data were corrected for mass dispersion. The results, normalized to one fission, were divided by the unfolded mass yield of Fraser *et al.*¹⁴ to give the x-ray yield per fragment. The unfolded x-ray yield per fragment is plotted as a solid line in Fig. 5 as a function of the pre-neutron-emission fragment mass. In order to show the effect of the unfolding process on the x-ray yield data, an uncorrected spectrum of the x-ray yield per fragment is plotted as a dashed line in Fig. 5. This spectrum was determined by dividing the x-ray yield by the fission-fragment yield for the appropriate mass before either distributions had been corrected for mass dispersion.

2. X-Ray Yield per Fragment as a Function of Mass

As was mentioned previously, the x-ray yields were measured from 1 to 56 nsec after fission. Glendenin and Unik,² using a somewhat similar detector configuration, measured the x-ray yields from the time of fission until 1 nsec after fission. The sum of both these x-ray yields should be similar to the x-ray yields measured by Kapoor *et al.*,¹ since they observed the fission fragments from the time of fission until 50 nsec after fission. All three distributions are plotted in Fig. 6 as a function of the post-neutron-emission fragment mass. Also shown in this graph is the Cf^{252} post-neutron-emission mass distribution reported by Fraser *et al.*¹⁴

The same general features can be observed in all three yield distributions shown in Fig. 6. The greatest discrepancies occur in the regions of low-mass yields,

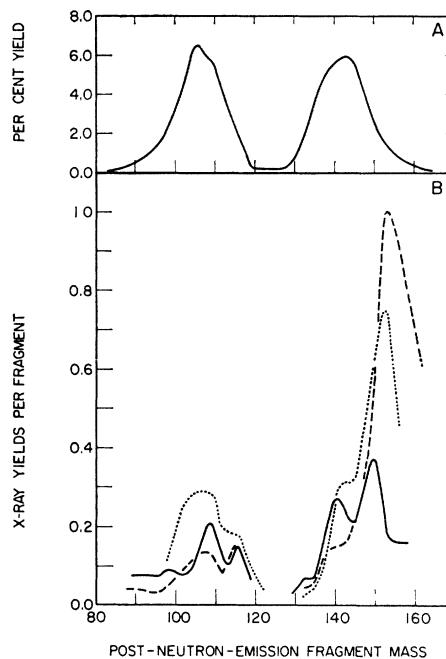


FIG. 6. (a) Fraser's (Ref. 14) time-of-flight Cf^{252} mass yields corrected for dispersion. (b) X-ray yields per fragment for Cf^{252} . The solid line is data from this experiment. The dashed line represents data reported by Glendenin (Ref. 2). The dotted line represents data reported by Kapoor (Ref. 1).

where the statistical uncertainties are the greatest. It should be pointed out that Kapoor made his measurements in a system that had a very different geometrical arrangement from this experiment. His solid angle was difficult to determine accurately, and his yields had to be corrected for the probability of x-ray transmission through a 0.5-mm-thick silicon detector.

The presence of more structure in the spectrum of the x-ray yields per fragment measured in this experiment can be attributed, in part, to the better signal-to-background ratio obtained with the geometric configuration that was used in this experiment. The positioning of a lead and copper shield between the x-ray detector and the source foil reduced the number of prompt γ rays and neutrons emitted at the time of fission, which normally produce a significant amount of coincidental background in the NaI crystal. Given these differences in the experimental systems that were used for recording the three different sets of data, it is unreasonable to expect the other measurements to show better agreement with the present experiment than is indicated.

3. X-Ray Yield per Fragment as a Function of Total Kinetic Energy

The x-ray data recorded during this experiment were also analyzed separately for the light and heavy fission fragments as a function of the total kinetic energy of both fragments. The same corrections as before were made for background, solid angle, detector efficiency, and absorption. The results were divided by the total

¹² A. H. Wapstra, G. J. Nygh, and R. Van Lieshout, *Nuclear Spectroscopy Tables* (North-Holland Publishing Co., Amsterdam, 1959).

¹³ J. Terrell, *Phys. Rev.* **127**, 880 (1962).

¹⁴ J. S. Fraser, J. C. D. Milton, H. R. Bowman, and S. G. Thompson, *Can. J. Phys.* **41**, 2080 (1963).

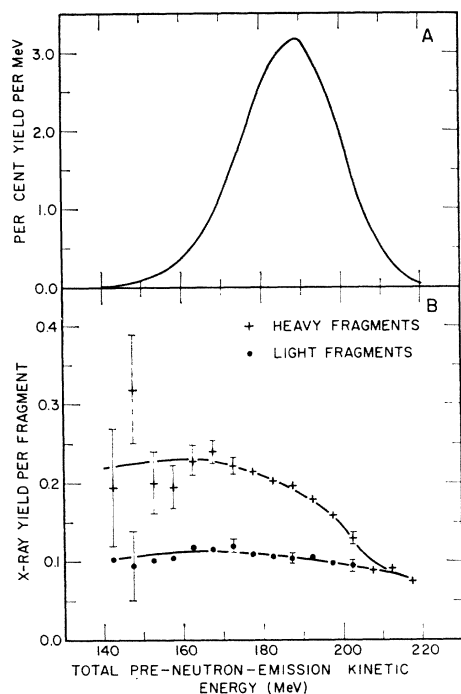


FIG. 7. (a) Total kinetic-energy yields for Cf^{252} measured in run 38 of the experiment. (b) X-ray yields per fragment for times between 1 and 56 nsec after fission of Cf^{252} for the light and heavy fragments.

number of fragments of the appropriate mass and energy group produced during the experiment to give the x-ray yield per fragment as a function of the total pre-neutron-emission kinetic energy for both the light and heavy fragments. A plot of these distributions, along with a graph of the total kinetic-energy yield measured during the experiment, is shown in Fig. 7.

C. X-Ray Times of Emission

1. Correction of the Timing Data

The time between the detection of a fission fragment in detector 1 and the detection of an x ray was measured by a time-to-pulse-height converter. By correcting the signal for the flight time of the fragment to detector 1, and the rise-time delay of the resulting pulse from the detector, the time that elapsed between fission and the detection of an x ray was obtained. The correction for the fragment's flight time was readily made, since the mass and kinetic energy of each fragment had been calculated. The rise-time correction was necessitated because the time required for the output of the fission-fragment detector to reach a voltage sufficient to trigger the time pickoff was a function of the pulse height of the signal. The following formula was used for the rise-time correction:

$$\Delta\tau_R = [V_{\text{disc}}/(a+bX)]\tau_R, \quad (2)$$

where τ_R is the rise time of the time pickoff (~ 5 nsec), V_{disc} is the discriminator level, and X is the measured

pulse height. The constants a and b relate the pulse height to the scale on which the discriminator setting was measured. It was found that these constants were dependent upon the bias voltage applied across the detector. No correction was necessary in the x-ray timing channel because of the high-gain fast-rise-time phototube that was used.

The corrected timing data were sorted according to the pre-neutron-emission mass of the fragment emitting the x ray into intervals 4 amu wide. The background was recorded as a function of the time after fission in a similar manner for the same mass intervals. The difference between these two measurements provided the data from which the analysis was made.

2. Prompt-Response Function

In order to determine the relative amount of different x-ray half-life groups that were present in the corrected-measured timing spectra, it was necessary to account for the prompt response of the system. This was done by deriving an analytical expression for the prompt-response function and then folding it into a sum of exponentials to give a function that could be fitted to the measured data. (See Ref. 15 for a more detailed explanation.)

Because of the high gain of the phototube, the timing equipment was triggered by the first photoelectron detected.¹⁶ Therefore, the probability of the photoelectron being detected at some time t greater than t_0 when the NaI was excited, was determined by Post and Schiff¹⁷ to be

$$D(t)dt = \tau_2^{-1} \exp[-(t-t_0)/\tau_2]dt, \quad (3)$$

$$\tau_2 = [(N_2+1)\lambda_2]^{-1} \quad (4)$$

where λ_2 is the decay constant of the scintillator and N_2 is the average total number of photons striking the phototube for a given x-ray excitation energy. By assuming that both the x-ray and the fission-fragment detectors had time responses of the form given by Eq. (3), it was possible to derive a function that represented the probability of a certain time elapsing between the production of the output pulses by two detectors observing a coincident event. This function was then folded with a Gaussian having a variance σ^2 to account for additional timing dispersion in the system. The resulting equation for the prompt-response function is

$$R(t) = \frac{1}{2}(\tau_1 + \tau_2)^{-1} [\exp(\frac{1}{2}\sigma^2/\tau_1^2 + t/\tau_1) \times \text{erfc}(\sigma/\sqrt{2}\tau_1 + t/\sqrt{2}\sigma) + \exp(\frac{1}{2}\sigma^2/\tau_2^2 - t/\tau_2) \times \text{erfc}(\sigma/\sqrt{2}\tau_2 - t/\sqrt{2}\sigma)], \quad (5)$$

where τ_1 and τ_2 correspond to the mean life associated with the fission fragment and x-ray detector, respectively, and t is measured from a time t_0 which is related

¹⁵ A. B. Long, B. W. Wehring, and M. E. Wyman (unpublished).

¹⁶ L. Bridwell and M. E. Wyman, Rev. Sci. Instr. **37**, 1145 (1966).

¹⁷ R. F. Post and L. I. Schiff, Phys. Rev. **80**, 1113 (1950).

to the time of the coincident event by the constant-time delays of the system.

The prompt response of the timing system that was used in the experiment was determined by studying the L x ray, which is emitted promptly by Cm^{248} after the α decay of Cf^{252} . The recorded timing distribution between the time of the α emission and the detection of an L x ray is shown in Fig. 8. Using different combinations of σ^2 , τ_1 , τ_2 , and t_0 , Eq. (5) was fitted to this distribution until a minimum for the sum of the weighted residuals was found. The values of the variables yielding this best fit are given at the top of Fig. 8, and the solid line in the figure was generated using these values.

The values for σ^2 and τ_1 cannot be readily compared with theoretically predicted values, since they result from a combination of the time dispersions introduced by the fission-fragment detector, the time pickoff, the fast phototube, and the time-to-pulse-height converter. However, this is not the case for τ_2 , since it is due to the long half-life state formed in the $\text{NaI}(\text{Tl})$ crystal.¹⁸ Therefore, Eq. (4) was used to calculate a value for τ_2 with $\lambda_2 = 4.44 \text{ sec}^{-1}$,¹⁹ and the value of N_2 , which was determined from the resolution of the x-ray detector for the 19-keV Cm^{248} L x ray.²⁰ The resulting value of $\tau_2 = 5.4 \pm 0.4 \text{ nsec}$ agreed well with the value of 5.88 that was determined in the fitting procedure.

3. Analysis of the Timing Spectra

The analysis of the measured x-ray timing data consisted of assuming a functional form for the unfolded

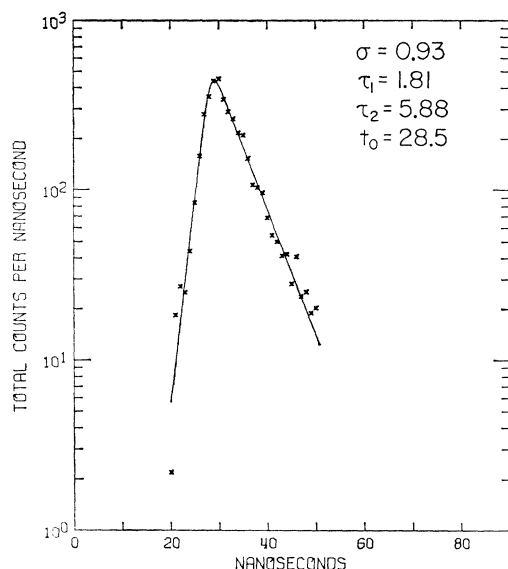


FIG. 8. Prompt-response function for the system. The distribution resulted from the measurement of the time of emission of a Cm^{248} L x ray after the α decay of Cf^{252} . The solid line is generated by fitting the prompt-response function to the measured data using the values of the parameters listed at the top of the figure.

¹⁸ A. Schwarzschild, Nucl. Instr. Methods 21, 1 (1963).

¹⁹ J. C. Robertson and J. G. Lynch, Proc. Phys. Soc. (London) 77, 751 (1961).

²⁰ R. K. Swank and W. L. Buck, Nucleonics 10, 51 (1952).

MASS INTERVAL 60 - 190

GROUP	AMOUNT	DECAY CONSTANT
1	24444.0	.600
2	22043.9	.100
3	11451.6	.010

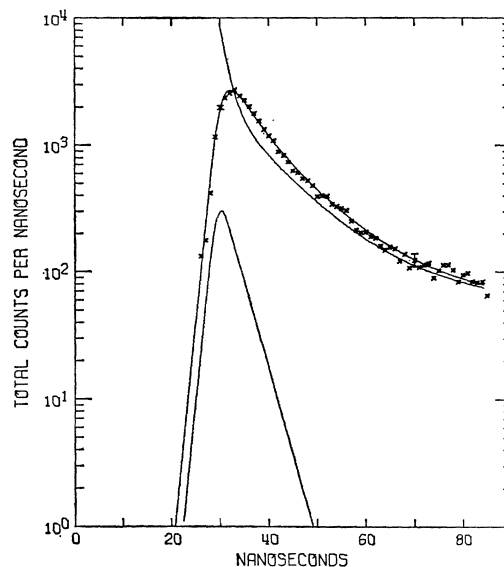


FIG. 9. Cf^{252} x-ray timing spectrum recorded for all mass fragments. The line drawn through the data points is the timing function fitted to the measured data. The unfolded function is the line which starts at a maximum and then decreases to follow below the fitted line. The prompt-response function is also shown in the figure.

spectrum and then folding in the analytical expression for the prompt-response function given in Eq. (5). The resulting function is fitted to the corrected measured data by varying certain parameters, which can then be interpreted in terms of the unfolded spectrum.

Because the x rays are emitted in less than 10^{-16} sec after internal conversion occurs, the timing data recorded in this experiment are a measurement of the decay characteristics of the excited fission-fragment nuclei. Therefore, one can assume that the unfolded spectrum may be represented by a sum of exponentials, each with a half-life of one of the nuclear transitions. Unfortunately, because of the possibility of many different transitions for each of the many different nuclei resulting from the fission of Cf^{252} , the sum would have too many terms to analyze. For this reason it was arbitrarily assumed that the timing data for each fission-fragment mass interval could be represented by a sum of three half-life groups, each with its own characteristic half-life. The justification for this scheme lay in the fact that the corrected timing data for every mass interval could be represented well by some combination of the same three half-life groups.

The folded distribution $F(t)$ may be expressed in terms of the prompt-response function $R(t)$ and the unfolded distribution $f(t)$ by

$$F(t) = \int_0^{\infty} f(t')R(t-t')dt', \quad (6)$$

where the unfolded distribution is assumed to have the

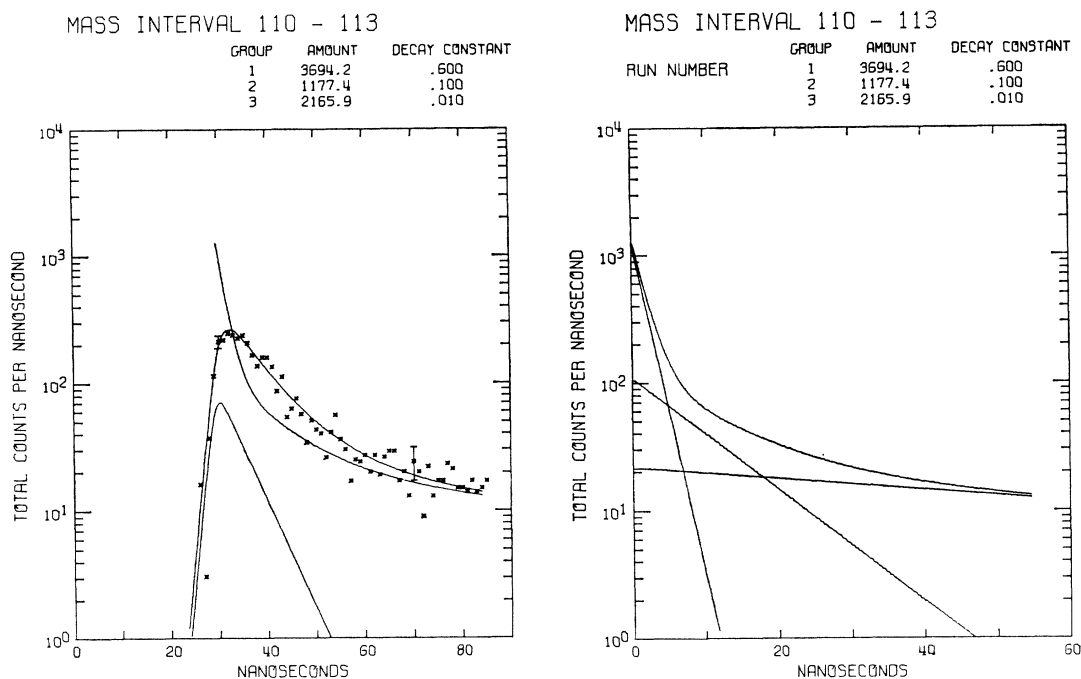


FIG. 10. X-ray timing data for pre-neutron-emission mass interval 110-113. The left-hand graph shows the corrected data points, the line generated by the fitted timing function, the line generated by the unfolded timing function and the prompt-response function. The right-hand graph shows the line generated by the unfolded timing function and the unfolded activities of each of the three half-life groups.

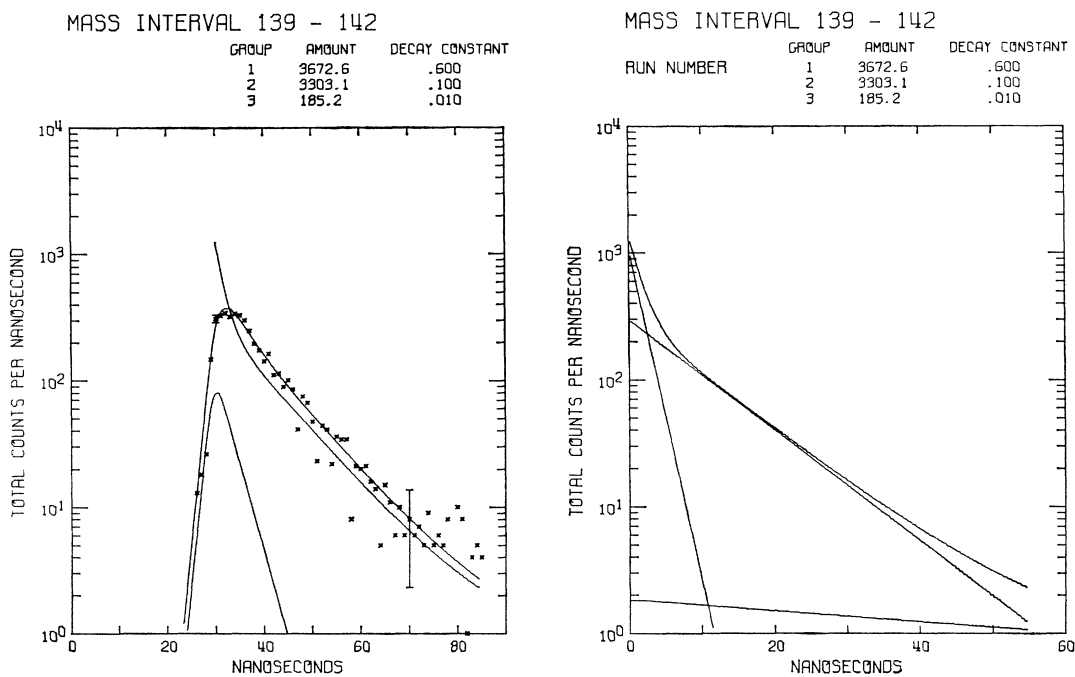


FIG. 11. X-ray timing data for pre-neutron-emission mass interval 139-142. The left-hand graph shows the corrected data points, the line generated by the fitted timing function, the line generated by the unfolded timing function and the prompt-response function. The right-hand graph shows the line generated by the unfolded timing function and the unfolded activities of each of the three half-life groups.

form

$$f(t') = \sum_{i=1}^3 A_i \exp(-\lambda_i t'). \quad (7)$$

Here λ_i and A_i are the decay constant and the activity of the i th half-life group. The result of performing the integration in Eq. (6), with the prompt-response function defined by Eq. (5), is

$$F(t) = \sum_{i=1}^3 \frac{1}{2} A_i (\tau_1 + \tau_2)^{-1} (\lambda_i + \tau_1^{-1})^{-1} \\ \times [\exp(\frac{1}{2}\sigma^2/\tau_1^2 + t/\tau_1) \operatorname{erfc}(\sigma/\sqrt{2}\tau_1 + t/\sqrt{2}\sigma) \\ + \exp(\frac{1}{2}\sigma^2\lambda_i^2 - \lambda_i t) \operatorname{erfc}(\sigma\lambda_i/\sqrt{2} - t/\sqrt{2}\sigma)] \\ - (\lambda_i - \tau_2^{-1})^{-1} [\exp(\frac{1}{2}\sigma^2/\tau_2^2 - t/\tau_2) \\ \times \operatorname{erfc}(\sigma/\sqrt{2}\tau_2 - t/\sqrt{2}\sigma) - \exp(\frac{1}{2}\sigma^2\lambda_i^2 - \lambda_i t) \\ \times \operatorname{erfc}(\sigma\lambda_i/\sqrt{2} - t/\sqrt{2}\sigma)]. \quad (8)$$

The value of the activity of each of the three half-life groups was determined by the weighted least-squares fitting of Eq. (8) to the corrected-measured timing data for a given mass interval. The values of the remaining parameters in Eq. (8) were determined in the following manner. From the measured prompt response, σ^2 and τ_1 were known, although it was found that τ_1 had to be adjusted to account for the difference between the surface-barrier detector's response to fission fragments and to α particles. The value of τ_2 was calculated, using Eq. (4), for the most probable K x-ray energy associated with a mass interval. The decay constants for the three half-life groups, which remained the same in the analysis of all the different mass intervals, were selected by systematically varying the λ_i 's until the best fit of Eq. (8) to the total timing spectra for all masses was obtained, as indicated by a minimum in the weighted sum of the residuals. A plot of the total timing spectrum for all masses is shown in Fig. 9. The solid line which closely follows the data points was generated with Eq. (8) by using the set of λ 's that gave the best fit and whose values are given at the top of the figure. These decay constants are representative of the entire measured time range and they yield a good fit to the timing data for each of the mass intervals considered in the present work.

The value of A_{ij} determined by this fitting process for the j th mass interval corresponds to the activity of the i th group at a time $t_{0x,j}$, which is also the time from which t is measured in Eq. (8) for this mass interval. The time $t_{0x,j}$ is related to the apparent time of fission t_f by the average time $\Delta t_{s,j}$ it takes for the fragments to move from the fission foil into the view of the x-ray detector:

$$t_{0x,j} = t_f + \Delta t_{s,j}. \quad (9)$$

The value of $\Delta t_{s,j}$ was determined from the average velocity of the fission fragments in the j th mass interval,

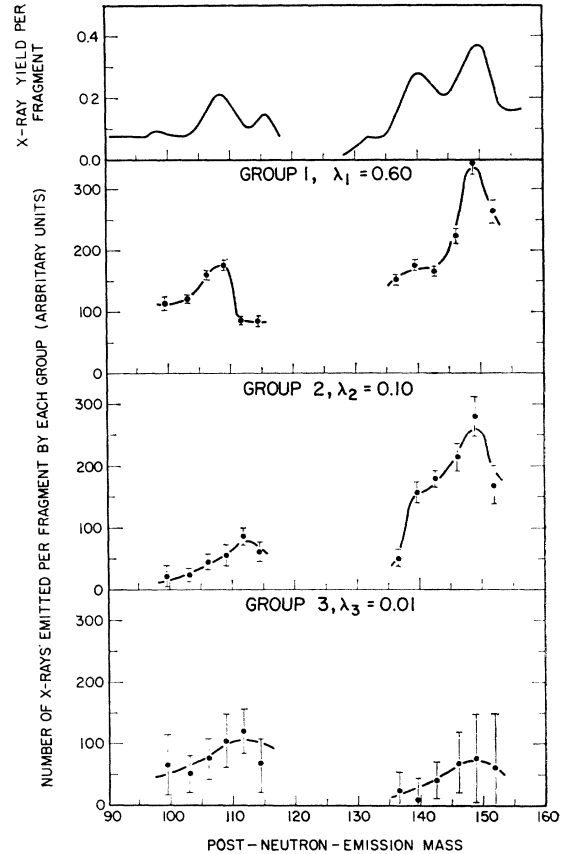


FIG. 12. Number of x rays emitted per fragment by each of the three half-life groups. This is plotted separately for each of the three half-life groups in the lower graphs on an arbitrary scale. The values of the λ 's are in nsec^{-1} . In the upper graph the x-ray yield per fragment measured between 1 and 56 nsec after fission is plotted.

and from the average distance traveled before the fragments came from behind the copper shield (Fig. 1) into the view of the x-ray detector. The value of the apparent time of fission corresponds to the value of t_0 measured for the prompt-response function and is displaced from the actual time of fission by the constant-timing delays in the system.

The timing data for two different mass intervals are presented in Figs. 10 and 11. In both cases, the fitted curves closely follow the data points, as can be seen in the left-hand graphs. Also shown on these graphs are the prompt-response functions generated for that mass interval. The unfolded timing curve is plotted in both the left- and right-hand graphs for each mass interval. In the left-hand graph, it is the line that starts at a maximum at a time equal to $t_{0x,j}$ and then decreases in magnitude following along below the fitted curve. In the right-hand graph it is plotted again, this time with the scale shifted so that $t_{0x,j}$ occurs at the origin. Also plotted in the right-hand graphs are the unfolded activities of each of the three half-life groups. The total numbers of x-ray emissions inherent in each group

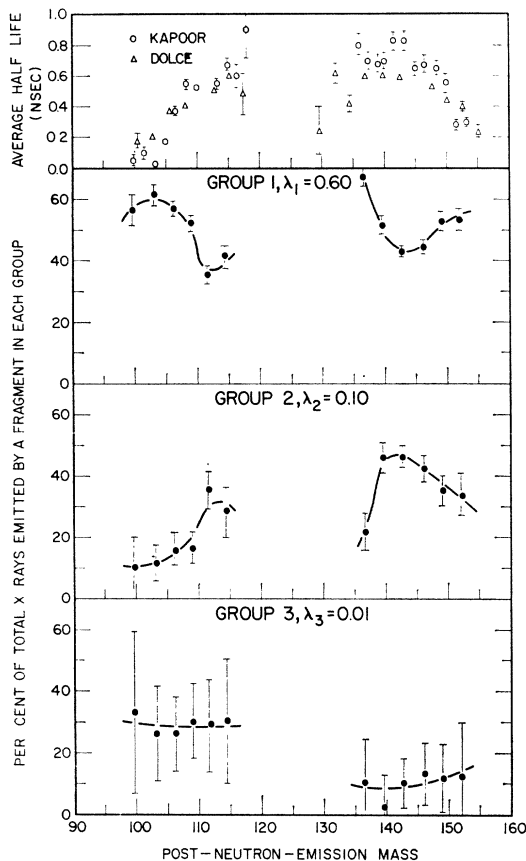


FIG. 13. Percent of the total x rays emitted per fragment that come from each of the three half-life groups. This is plotted separately for each of the three half-life groups in the lower graphs. The values of the λ 's are in nsec^{-1} . In the upper graph the average half-life for x-ray emission is plotted as a function of fragment mass. The values were reported by Dolce (Ref. 6) and by Kapoor (Ref. 1).

from the time of fission to infinity, as defined by N_{ij} in

$$N_{ij} = (A_{ij}/\lambda_{ij}) \exp(\lambda_{ij}\Delta t_{s,j}) \quad (10)$$

is printed at the top of each graph. By comparing these values and the shapes of the folded distributions in Figs. 10 and 11, it is possible to observe the difference in the timing spectra recorded for mass intervals 110–113 and 139–142.

4. Times of X-Ray Emission as a Function of Fragment Mass

The use of the fitting technique described in the preceding section greatly simplified the analysis of the data, and it enabled the final results to be presented succinctly in terms of the total number of x rays that were emitted in each of the three half-life groups by a fragment from 1 of the 12 mass intervals analyzed. The results are plotted in Fig. 12 on a relative scale versus the most probable post-neutron-emission mass of each interval. Also plotted in Fig. 12 is the unfolded x-ray yield per fragment.

In order to exhibit the relative contribution of each of the three half-life groups to the total x-ray emissions for a given mass interval, the percent of the total emissions occurring in each of the three half-life groups was plotted, in Fig. 13, versus the most probable post-neutron-emission mass for each of the 12 intervals. Plotted at the top of Fig. 13 are the average half-lives that were previously reported by Dolce for Cf^{252} x-ray emission from the time of fission to 4 nsec after,⁶ and by Kapoor for Cf^{252} x-ray emission from the time of fission to 2 nsec after.¹ Because of the difference in the time region investigated in those experiments and in the present work, only a superficial comparison can be made between the results. In general, it is seen that a mass interval in which a large percent of the x-ray emissions occur in the shortest half-life group is an interval in which they have recorded a short average half-life. Similarly, a mass interval having a small percent of the x-ray emissions in the shortest half-life group corresponds to a mass for which they have measured a long average half-life.

The error bars shown in Figs. 12 and 13 indicate the uncertainties associated with the values of the N_{ij} 's due to the process of fitting a function to data points that have statistical uncertainties. The method for determining these uncertainties is described by Hildebrand.²¹ Any errors that might be present due to

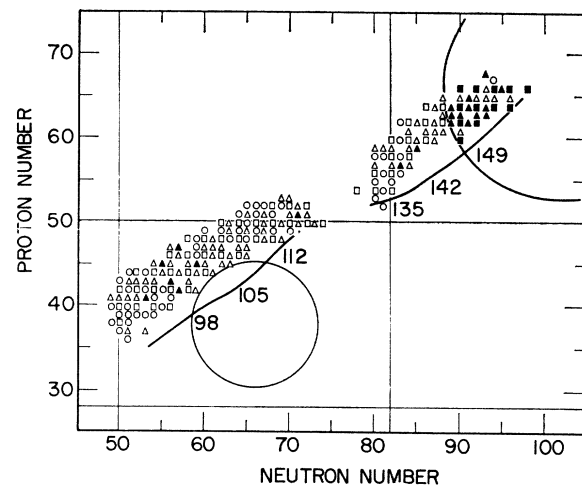


FIG. 14. Graph of nuclides showing the relationship of the Cf^{252} fission fragments to nuclides for which experimental data have been accumulated. Even-even nuclei, with a level having $\tau < 10^{-10}$ sec, are shown by (\square); even-even nuclei, $\tau \approx 2 \times 10^{-9}$ sec, (\blacksquare); nuclei with no energy level below 200 keV, (\circ); nuclei with less than three energy levels below 200 keV, (\triangle); and nuclei with three or more energy levels below 200 keV, (\blacktriangle). The most probable neutron and proton number for a given Cf^{252} fragment mass is indicated by the solid line falling just below the reported data. Horizontal and vertical lines are drawn at the magic proton and neutron numbers, respectively, and the regions of expected deformed nuclei are enclosed within the circular lines.

²¹ F. B. Hildebrand, *Introduction to Numerical Analysis* (McGraw-Hill Book Co., New York, 1956).

uncertainties in the parameters used in Eq. (8) are not included, because they would be systematically present in all the N_{ij} 's and, therefore, would have a small effect on the results that are drawn from comparisons of these values.

IV. DISCUSSION OF RESULTS

The K x rays that are detected within the time range of this experiment result primarily from the internal conversion of $E2$ and $M1$ transitions of less than 200 keV.²² In order to exhibit the nuclear regions from which large x-ray yields might be expected, data that have been reported on nuclear structure^{22,23} were plotted in Fig. 14 in terms of the number of known nuclear levels below 200 keV. It is necessary to extrapolate this information to the regions of the fission-fragment nuclei, which are indicated in Fig. 14 as lines generated from the most probable post-neutron-emission Cf²⁵² fragment masses.

A general comparison between the light- and heavy-fragment timing results that are shown in Figs. 12 and 13 indicates that x-ray emissions from the longest half-life group account for a larger percentage of the total emissions by the light fragments than by the heavy. This same effect was reported for the thermal fission of U²³⁵ and Pu²³⁹ by Bridwell.²⁴ On the other hand, a marked similarity may be observed in the detailed structure of the x-ray timing and yield data measured for the light and for the heavy fragments by comparing the results for the light fragments, as their mass is decreased from the closed proton shell at mass 122, with those for the heavy fragments, as their mass is increased from the closed neutron shell at mass 135. Near the magic proton or neutron numbers, the x-ray yield per fragment is small and due mostly to the shortest half-life group $\lambda_1=0.6$ nsec⁻¹, as can be seen in Fig. 13. This is to be expected for magic nuclei, since the energy level of the first excited state is generally high, and, therefore, the probability of a transition from this level internally converting is small and its life time is short.

However, shifting to consider fragments whose masses

lie in the region of the spherical nuclei, it is found that the energy of the excited levels tend to decrease.²⁵ The presence of more energy levels below 200 keV in this mass range can be used to explain the increase in x-ray yield that is observed in Figs. 12 and 13 as mostly due to the longer half-life groups.

In the deformed region, experimental data indicate that the number of energy levels below 200 keV increases substantially.^{22,23,25} This is reflected by a corresponding increase in the x-ray yields per fragment as both the light and heavy fragments enter the regions of expected deformed nuclei. In the case of the heavy fragments, part of the x-ray-yield increase in the shortest half-life group can be attributed to even-even nuclei. This is due to a decrease in the energy level of the first excited state for even-even nuclei having more than 90 neutrons, which increases the probability of internal conversion and raises the transition half-life to approximately 1 nsec.²³

The increase in the x-ray yield per fragment as the light fragments enter the expected region of deformed nuclei, however, cannot be attributed to the even-even nuclei. In order to explain why this increase in yield also comes mostly from the shortest half-life group (Fig. 12), it has been suggested that a collective enhancement of the many different low-lying energy levels might result in a shorter half-life.⁶

The final effect is a sharp decrease in the x-ray yields for fragments whose masses lie within the region of expected deformed nuclei. There have been two theories proposed to explain this effect^{2,26}; however, neither one appears to be satisfactory for both the light and the heavy fragments. It is hoped that experimental information about the energy of the transitions involved will resolve the question.

ACKNOWLEDGMENTS

The authors would like to express their appreciation to P. Axel, E. Bohn, L. J. Koester, and C. W. Williams for their helpful discussions on various aspects of this work. The authors are also indebted to S. Hinata, D. Lerche, and R. Rollins for their assistance with the experiment, and to R. Harrison and J. Goldman for construction of the vacuum chambers.

²² C. M. Lederer, J. M. Hollander, and I. Perlman, *Table of Isotopes* (John Wiley & Sons, Inc., New York, 1967).

²³ P. H. Stelson and L. Grodzins, *Nucl. Data* **1**, A21 (1965).

²⁴ L. Bridwell, M. E. Wyman, and B. W. Wehring, *Phys. Rev.* **145**, 963 (1966).

²⁵ R. Sheline, *Rev. Mod. Phys.* **32**, 1 (1960).

²⁶ R. A. Atneosen, T. D. Thomas, W. M. Gibson, and M. L. Perlman, *Phys. Rev.* **148**, 1206 (1966).